Published in final edited form as:

Nature. 2021 April ; 592(7852): 116–121. doi:10.1038/s41586-020-2895-3.

Spike mutation D614G alters SARS-CoV-2 fitness

Jessica A. Plante[#1,2,3], **Yang Liu**[#4], **Jianying Liu**[#2,3], **Hongjie Xia**[4], **Bryan A. Johnson**[2], **Kumari G. Lokugamage**[3], **Xianwen Zhang**[4], **Antonio E. Muruato**[2,3], **Jing Zou**[4], **Camila R. Fontes-Garfias**[4], **Divya Mirchandani**[1,2,3], **Dionna Scharton**[1,2,3], **John P. Bilello**[5], **Zhiqiang Ku**[6], **Zhiqiang An**[6], **Birte Kalveram**[7], **Alexander N. Freiberg**[2,7,9,10], **Vineet D. Menachery**[2,3], **Xuping Xie**[4,#], **Kenneth S. Plante**[1,2,3,#], **Scott C. Weaver**[1,2,3,8,9,10,#], **Pei-Yong Shi**[4,8,9,10,11,12,#]

[1]World Reference Center for Emerging Viruses and Arboviruses, University of Texas Medical Branch, Galveston TX, USA

[2]Institute for Human Infections and Immunity, University of Texas Medical Branch, Galveston TX, USA

[3]Department of Microbiology and Immunology, University of Texas Medical Branch, Galveston TX, USA

[4]Department of Biochemistry and Molecular Biology, University of Texas Medical Branch, Galveston TX, USA

[5]Gilead Sciences, Inc., Foster City, CA, USA

[6]Texas Therapeutics Institute, Brown Foundation Institute of Molecular Medicine, University of Texas Health Science Center at Houston, Houston, USA

[7]Department of Pathology, University of Texas Medical Branch, Galveston TX, USA

[8]Institute for Translational Sciences, University of Texas Medical Branch, Galveston, TX, USA

[9]Center for Biodefense & Emerging Infectious Diseases, University of Texas Medical Branch, Galveston, TX, USA

[10]Sealy Institute for Vaccine Sciences, University of Texas Medical Branch, Galveston, TX, USA

[11]Sealy Center for Structural Biology & Molecular Biophysics, University of Texas Medical Branch, Galveston, TX, USA

[12]Lead Contact

[#]Correspondence: X.X. (xuxie@UTMB.edu), K.S. P. (ksplante@utmb.edu), S.C.W. (sweaver@utmb.edu), or P.-Y.S. (peshi@UTMB.edu).

Author contributions

Conceptualization, Y.L., V.D.M., X.X., K.S.P., S.C.W., P.-Y.S.; Methodology, J.A.P, Y.L., J.L., H.X., B.A.J., K.G.L., X.Z., A.E.M., J.Z., C.R.F.G., A.N.F., V.D.M., X.X., K.S.P., S.C.W., P.-Y.S.; Investigation, J.A.P, Y.L., J.L., H.X., B.A.J., K.G.L., X.Z., A.E.M., J.Z., C.R.F.G., D.M., D.S., J.P.B., A.N.F., V.D.M., X.X., K.S.P., S.C.W., P.-Y.S.; Resources, Z.K., Z.A.; Data Curation, J.A.P, Y.L., J.L., H.X., B.A.J., K.G.L., X.Z., A.E.M., J.Z., A.N.F., V.D.M., X.X., K.S.P.S.C.W., P.-Y.S.; Writing-Original Draft, J.A.P, Y.L., J.L., X.X., K.S.P., S.C.W., P.-Y.S; Writing-Review & Editing, J.A.P, Y.L., J.L., H.X., B.A.J., K.G.L., X.Z., A.E.M., J.Z., A.N.F., V.D.M., X.X., K.S.P., S.C.W., P.-Y.S.; Supervision, A.N.F., V.D.M., X.X., K.S.P., S.C.W., P.-Y.S.; Funding Acquisition, A.N.F., V.D.M., S.C.W., P.-Y.S..

Competing financial interests

X.X., V.D.M., and P.-Y.S. have filed a patent on the reverse genetic system and reporter SARS-CoV-2. Other authors declare no competing interests.

# These authors contributed equally to this work.

Summary

A spike protein mutation D614G became dominant in SARS-CoV-2 during the COVID-19 pandemic[1,2]. However, the impact on viral spread and vaccine efficacy remains to be defined. Here, we engineer the D614G mutation in the USA-WA1/2020 strain and characterize its effect. D614G enhances replication on human lung epithelial cells and primary human airway tissues through an improved infectivity of virions. Hamsters infected with the G614 variant produced higher infectious titers in the nasal washes and trachea, but not lungs, confirming clinical evidence that the D614G mutation enhances viral loads in the upper respiratory tract of COVID-19 patients and may increases transmission. Sera from D614-infected hamsters exhibit modestly higher neutralization titers against G614 virus than against D614 virus, indicating that (i) the mutation may not reduce the ability of vaccines in clinical trials to protect against COVID-19 and (ii) therapeutic antibodies should be tested against the circulating G614 virus. Together with clinical findings, our work underscores the importance of this mutation in viral spread, vaccine efficacy, and antibody therapy.

Introduction

Since the emergence of severe acute respiratory syndrome coronavirus 2 (SARS-CoV-2) in China in late 2019[3], coronavirus disease 2019 (COVID-19) has caused >36 million confirmed infections and >1 million fatalities worldwide. Although most infections are mild, SARS-CoV-2 can cause severe, life-threatening pneumonia, particularly in older age groups and those with chronic conditions. The exact mechanisms of severe disease remain unclear but typically involve a dysregulated, hyperinflammatory response following viral infection[4]. However, in addition to the host response, variation in viral strain could contribute to disease severity and spread efficiency.

Coronaviruses have evolved a genetic proofreading mechanism to maintain their long RNA genomes[5]. Despite the low sequence diversity of SARS-CoV-2[6], mutations in the spike protein, which interacts with cellular receptors such as angiotensin-converting enzyme 2 (ACE2) to mediate entry into cells, can strongly influence host range, tissue tropism, and pathogenesis. During the SARS-CoV outbreak in 2002–2003, one such mutation mediated adaptation for infection of the intermediate civet host as well as interhuman transmission[7]. For SARS-CoV-2, analyses of over 28,000 spike gene sequences in May 2020 revealed a D614G amino acid substitution that was rare before March but increased in frequency as the pandemic spread[1], reaching over 74% of all published sequences by June 2020[2]. The D614G substitution was accompanied by three other mutations: a C-to-T mutation in the 5’ untranslated region at position 241, a synonymous C-to-T mutation at position 3,037, and a nonsynonymous C-to-T mutation at position 14,408 in the RNA-dependent RNA polymerase gene[8]. This set of mutations not only increased globally, but during co-circulation within individual regions during outbreaks, suggesting a fitness advantage rather than founder effects or genetic drift. The association of spike amino acid substitutions with coronavirus transmissibility suggested that the D614G substitution was critical to this putative selective sweep. The correlation of this mutation with higher nasopharyngeal viral

RNA loads in COVID-19 patients[1,9] also supported a putative advantage of the mutant in transmission. However, direct measurements of fitness were needed to confirm this hypothesis.

Initial phenotypic characterizations of the D614G spike substitution were performed using pseudotyped viruses, whereby vesicular stomatitis virus (VSV) and lentiviral particles incorporating the SARS-CoV-2 spike protein were studied by replication kinetics. The production of significantly higher pseudotyped viral titers in multiple cell types suggested that G614 could be associated with enhanced entry into cells and replication in airways[1,2]. However, these results need to be confirmed in studies with authentic SARS-CoV-2 containing the D614G variant, and also using *in vivo* studies with a suitable animal model. Therefore, using an infectious cDNA clone for SARS-CoV-2[10], we generated the D614G substitution in the USA-WA1/2020 strain[11] and performed experimental comparisons using *in vitro* cell culture, primary human 3D airway tissue, and a hamster infection model[12]. We also developed D614 and G614 mNeonGreenSARS-CoV-2 viruses for rapid neutralization testing of serum specimens and monoclonal antibodies (mAbs). Our study has important implications in understanding the evolution and transmission of SARS-CoV-2 as well as the development of COVID-19 vaccines and therapeutic antibodies.

Results

Enhancement of viral replication and infectivity by the spike D614G substitution in human lung epithelial cells.

We first examined the effect of the spike D614G substitution on viral replication in cell culture. A site-directed mutagenesis was performed on an infectious cDNA clone of SARS-CoV-2 to prepare a pair of recombinant isogeneic viruses with spike D614 or G614 (Fig. 1a). Similar infectious amounts of D614 and G614 viruses were recovered from Vero E6 cells (monkey kidney epithelial cells). The two viruses formed similar plaque morphologies (Fig. 1b). In Vero E6 cells, the G614 virus replicated to a higher infectious titer than D614 at 12 h post-infection (hpi), after which the two viruses replicated to comparable levels (Fig. 1c). A similar trend was observed for extracellular viral RNA production from the infected Vero E6 cells (Fig. 1d). Sequencing of the spike gene of the Vero E6-derived viruses did not reveal any undesired mutations. To compare the infectivity between the two viruses, we calculated the genomic RNA/PFU ratios; no significant differences were found (Fig. 1e), indicating that the D614G mutation does not affect viral replication or virion infectivity in Vero E6 cells.

Next, we compared the replication kinetics of D614 and G614 viruses on human lung epithelial Calu-3 cells. With a multiplicity of infection (MOI) of 0.01, the G614 virus produced modest 1.2-, 2.4-, and 1.9-fold more infectious virus than the D614 virus at 24, 36, and 48 hpi, respectively (Fig. 1f), indicating that D614G enhances viral replication. In contrast, the G614-infected cells produced less (at 24 and 36 hpi) or equivalent (at 48 hpi) extracellular viral RNA compared to D614-infected cells (Fig. 1g). The genomic RNA/PFU ratios of D614 virus were therefore 1.9- to 3.0-fold higher than those of G614 (Fig. 1h), indicating that the D614G mutation increases the infectivity of SARS-CoV-2 produced from a human lung cell line.

To explore the mechanism of increased infectivity of G614 virus produced from Calu-3 cells, we compared the spike protein processing from D614 and G614 viruses. Virions were purified from the culture medium of infected Calu-3 using ultracentrifugation and a sucrose cushion. The pelleted viruses were analyzed for spike protein processing by Western blot, with nucleocapsid included as a loading control. For both viruses, full-length spike was almost completely processed to the S1/S2 cleavage form and S2', with comparable cleavage efficiencies of 93% for D614 and 95% for G614 (Fig. 1i). When virions produced from Vero E6 cells were analyzed, less full-length spike protein was processed to the S1/S2 form, with cleavage efficiencies of 73% for D614 and 67% for G614 (Fig. 1j). Uncropped images are available in Supplementary Fig. 1. These results suggest that (i) more spike protein is cleaved to S1/S2 within virions produced from Calu-3 cells compared to Vero E6 cells and (ii) the D614G substitution does not significantly affect the spike cleavage ratio.

Increased fitness in the hamster upper airway of SARS-CoV-2 with theD614G substitution.

The *in vivo* relevance of the D614G mutation was evaluated in the golden Syrian hamster model (Extended Data Fig. 1a). After intranasally infecting four-to five-week-old hamsters with 2×10^4 PFU of D614 or G614 virus, animals from both groups exhibited similar weight loss (Fig. 2a). On day 2 post-infection (pi), infectious viral titers from nasal washes, trachea, and various lobes of the lung (Extended Data Fig. 1b) were consistently higher in the G614-infected subjects compared to the D614-infected animals, especially in the upper airway, although the differences did not reach statistical significance (Fig. 2b). On day 4 pi the differences in infectious viral titers became more pronounced in the upper airway, with $1.3\log_{10}$ PFU/ml higher G614 virus than D614 in nasal wash and $0.9\log_{10}$ PFU/g in the trachea (Fig. 2c). Viral loads in the lung were essentially identical. No infectious virus was detected on day 7 pi (data not shown).

We compared the infectivity of the D614 and G614 viruses produced in hamsters by determining their viral RNA levels and viral RNA/PFU ratios. The two viruses produced nearly identical levels of viral RNA across all organs and timepoints (Fig 2d). The RNA/PFU ratios of G614 virus were $0.3\log_{10}$ to $0.7\log_{10}$ lower than those of D614 virus across airway tissues on day 2 pi (Fig. 2e). On day 4 pi, the RNA/PFU ratio of G614 was $1.1\log_{10}$ lower than that of D614 in nasal wash, while the differences in the trachea and lungs were negligible (Fig. 2f). On day 7 pi, despite no detectable infectious virus (detection limit 40 PFU/ml), more than 10^8 viral genomes/ml were detected in the nasal washes (Fig. 2d), demonstrating high levels of viral RNA persistence after the clearance of infectious virus. This result recapitulates findings in COVID-19 patients, who frequently test positive with RT-PCR for up to several weeks but have low or undetectable infectious virus. One caveat of the above calculations is that the total RNA could include viral RNAs from both virions and cells lysed during sample processing.

The above results prompted us to directly compare the finesses of D614 and G614 viruses through a competition experiment. This approach has major advantages over performing individual strain infections with numerous host replicates; each competition is internally controlled, eliminating host-to-host variation that can reduce the power of experiments, and the virus strain ratios can be assayed with more precision than individual virus titers. Thus,

competition assays have been used for many studies of microbial fitness, including viruses[13–16]. Hamsters were infected intranasally with equal amounts of the two viruses (10^4 PFU per virus). On days 2, 4, and 7 pi, nasal wash and respiratory organs were harvested and quantified for relative amounts of D614 and G614 RNAs by RT-PCR and Sanger sequencing. This method was validated to reliably quantify the relative amounts of D614 and G614 viruses in a mixed specimen (Extended Data Fig. 2). A G614/D614 ratio of >1.0 indicates a replication advantage for G614. All respiratory tissues showed G614/D614 ratios of 1.2 to 2.6 on days 2, 4, and 7 pi, indicating that G614 virus has a consistent advantage over D614 virus (Fig. 2g–i).

Dramatic enhancement of viral replication by spike mutation D614Gin a primary human airway tissue model.

To further define the function of D614G mutation inhuman respiratory tract, we characterized the replication of D614 and G614 viruses in a primary human airway tissue model (Fig. 3a). This airway model contains human tracheal/bronchial epithelial cells in multilayers which resemble the epithelial tissue of the respiratory tract. The primary tissue is cultured at an air-liquid interface to recapitulate the barrier, microciliary response, and infection of human airway tissues *in vivo*[17,18]. After infecting the airway tissue at an MOI of 5 (as determined on Vero E6 cells), both D614 and G614 viruses produced increasing infectious titers from day 1 to 5, up to 7.8×10^5 PFU/ml (Fig. 3b), demonstrating that the airway tissue supports SARS-CoV-2 replication. The infectious viral titers of G614 were significantly higher (2.1- to 8.6-fold) than those of D614 (Fig. 3b). In contrast, no differences in viral RNA yields were observed (Fig. 3c). The genomic RNA/PFU ratios of D614 virus were 1.4- to 5.3-fold higher than those of G614 virus (Fig. 3d). Sequencing of the viruses collected on day 5 pi did not show any acquired mutations. Collectively, the results demonstrate that G614 enhances viral replication through increased virion infectivity in primary human upper airway tissues.

Next, we performed competition experiments in the human airway culture. After infecting with a 1:1 infectious ratio of D614 and G614 viruses, the G614/D614 ratios increased from 1.2 at 1 dpi to 13.9 at 5 dpi (Fig. 3e). In addition, after infecting the airway culture with 3:1 ratio of D614 and G614 viruses, the G614 variant rapidly overcame its initial deficit to reach a slight advantage with a G614/D614 ratio of 1.2 by day 1 pi, with that advantage increasing to 9.1 by 5 dpi (Fig. 3f). Furthermore, when infecting the airway tissue with a 9:1 ratio of D614 to G614, the G614/D614 ratios increased from1.4 to 5.2 from days 1 to 5 pi (Fig. 3g). A similar competition result was obtained when the experiment was repeated using a different donor-derived human airway culture (Extended Data Fig. 3). These results confirm that the G614 virus can rapidly outcompete the D614 virus when infecting human airway tissues, even as an initially minor variant in a mixed population.

Stability of D614 and G614 viruses.

To examine the effect of D614G on virus stability, we measured the decay of infectivity of D614 and G614 viruses over time at 33°C, 37°C, and 42°C (Extended Data Fig. 4). The infectivity of both viruses decreased at a faster rate at 42°C than at 37°C or 33°C. However,

the G614 virus retained higher infectivity than the D614 virus at all temperatures, suggesting that the D614G mutation may increase the stability of SARS-CoV-2.

Effect of spike mutation D614G on neutralization susceptibility.

All of the COVID-19 vaccines currently in clinical trials are based on the original D614 spike sequence[19,20]. An important question is whether the D614G substitution could reduce vaccine efficacy, assuming G614 virus continues to circulate. To address this question, we measured the neutralization titers of a panel of sera collected from hamsters that were previously infected with D614 SARS-CoV-2 (Extended Data Fig. 5). Each serum was analyzed by a pair of mNeonGreen reporter SARS-CoV-2 viruses with either the D614 or the G614 spike (Extended Data Fig. 6)[21]. The mNeonGreen gene was engineered at the open-reading-frame 7 of the SARS-CoV-2 genome[10]. As shown in Figs. 4a–c, all sera exhibited 1.4- to 2.3-fold higher neutralization titers (mean 1.7-fold) against heterologous G614 virus compared to homologous D614 virus (Extended Data Fig. 7), suggesting that mutation D614G may confer higher susceptibility to serum neutralization.

Next, we evaluated a panel of eleven human receptor-binding domain (RBD) mAbs against the D614 and G614 mNeonGreen SARS-CoV-2 viruses. The details of these RBD mAbs are reported elsewhere (An et al., submitted for publication). One mAb (mAb18) showed a 2.1-fold higher potency against G614 than D614 virus, whereas the other ten mAbs exhibited similar neutralization activities against both viruses (Figs. 4d–f and Extended Data Figs. 8 and 9). The results suggest that mutation D614G may modulate spike protein conformation to affect mAb neutralization in an epitope-specific manner.

Discussion

We demonstrated that the spike substitution D614G enhanced SARS-CoV-2 replication in the upper respiratory tract through increased virion infectivity. Compared with the original D614 virus, the emergent G614 virus replicated to a higher level in the human lung Calu-3 cells and primary human upper airway tissues. The replication differences were more dramatically observed in the human airway culture, with up to a 13.9-fold advantage in a head-to-head competition test. The increased replication fitness correlated with an enhanced specific infectivity and stability of the G614 virions. Since previous studies with pseudotyped virus showed that the cleavage efficiency of the spike protein into S1/S2 modulates SARS-CoV-2 infection[22,23], we compared the spike cleavage ratios between the D614 and G614 virions. Although virions produced from Calu-3 cells had more complete S1/S2 cleavage than those produced form Vero E6 cells, no substantial differences in spike cleavage were detectable between the D614 and G614 virions, suggesting that the enhanced virion infectivity is not likely due to a D614G-mediated spike cleavage difference. Our results from authentic SARS-CoV-2 are in contrast with previous studies reporting that the D614G mutation changes the cleavage and shedding of spike protein when expressed alone on pseudotyped virions[24,25]. Mechanistically, recent studies showed that the D614G mutation abolishes a hydrogen-bond interaction with T859 from a neighboring protomer of the spike trimer[1], which allosterically promotes the RDB domain to an “up” conformation for receptor ACE2 binding[2], leading to an enhanced virion infectivity.

The higher viral loads of G614 in the upper airway of COVID-19 patients[26] and infected hamsters suggest the role of D614G mutation in viral transmissibility. The robust replication of SARS-CoV-2 in the human upper airway may be partially conferred by a higher ACE2 receptor expression in the nasal cavity compared to the lower respiratory tract[8,27]. Compared with D614, the G614 virus replicated to a higher level in the upper airway, but not in the lungs, of hamsters, suggesting that the D614G mutation may select against lung replication. In clinics, patients with G614 virus developed higher levels of viral RNA in nasopharyngeal swabs than those with D614 virus, but did not develop more severe disease[1,2,9]. Our hamster infection model recapitulated these clinical findings: the G614 virus developed higher infectious titers than the D614 virus in nasal washes and tracheas, but not lungs, and no differences in weight loss or signs of disease were observed. If the lower viral RNA/PFU ratio of the G614 virus observed in our hamster and human airway models could be extrapolated to COVID-19 patients, the modest differences in cycle threshold [28] values observed in patients' nasopharyngeal swabs would translate to ≥10-fold more infectious G614 virus, underscoring the potential for enhanced transmission and spread. Indeed, during the revision of our publication, Hou and colleagues posted a non-peer-reviewed manuscript reporting that G614 mutation increased SARS-CoV-2 transmission in hamsters[29]. This potential is further bolstered by the observation that a COVID-19 patient with distinct populations of SARS-CoV-2 in throat swabs and sputum samples only transmitted the throat strain[26]. Similar nasal-driven transmission was recently reported for human influenza A virus in ferrets[30]. However, age-dependent impacts of D614G on SARS-CoV-2 infection, pathogenesis, and transmission remain to be studied.

G614 virus was modestly more susceptible to neutralization by sera collected from D614 virus-infected hamsters. This seems counterintuitive, but could be explained by a D614G-mediated increase in the "up" conformation of the RDB[1,2]. Since current COVID-19 vaccines in clinical trials are based on the original D614 sequence, our neutralization result mitigates the concern that the D614G mutation might compromise their efficacy. Future studies are needed to eliminate this concern by testing human sera collected from D614 spike vaccinees. Besides antisera, we also showed that, depending on the epitope locations on RBD, the neutralizing potency of certain mAbs may be affected by the D614G mutation. The results underscore the importance to test therapeutic mAbs against G614.

In summary, we have used authentic SARS-CoV-2 to demonstrate that spike substitution D614G enhances viral replication in the upper respiratory tract and increases neutralization susceptibility. These findings have important implications in understanding the evolution and spread of the ongoing COVID-19 pandemic, vaccine efficacy, and therapeutic antibody development. Future efforts are warranted to study other emerging mutations, including those that accompanied with the D614G substitution in SARS-CoV-2.

Methods

Ethics statement.

Hamster studies were performed in accordance with the guidance for the Care and Use of Laboratory Animals of the University of Texas Medical Branch (UTMB). The protocol was approved by the Institutional Animal Care and Use Committee (IACUC) at UTMB. All the

hamster operations were performed under anesthesia by isoflurane to minimize animal suffering.

Animals and Cells.

The Syrian hamsters (HsdHan:AURA strain) were purchased from Envigo (Indianapolis, IN). African green monkey kidney epithelial Vero E6 cells (kindly provided by Ralph Baric, University of North Carolina) were grown in Dulbecco's modified Eagle's medium (DMEM) with 5% fetal bovine serum (FBS; HyClone Laboratories, South Logan, UT) and 1% antibiotic/streptomycin (Gibco). Human lung adenocarcinoma epithelial Calu-3 cells (ATCC, Manassas, VA) were maintained in a high-glucose DMEM supplemented with 10% FBS and 1% penicillin/streptomycin at 37°C with 5% CO_2. The EpiAirway system is a primary human airway 3D tissue model purchased from MatTek Life Science (Ashland, MA). This EpiAirway system was maintained with the provided culture medium at 37°C with 5% CO_2following the manufacturer's instruction. All other culture medium and supplements were purchased from ThermoFisher Scientific (Waltham, MA). All cell lines were verified and tested negative for mycoplasma. No further authentication of cell lines was performed.

Generation of SARS-CoV-2 spike D614G mutant viruses.

One single-nucleotide substitution was introduced into a subclone puc57-CoV-2-F5–7 containing the spike gene of the SARS-CoV-2 wild type (WT) infectious clone[10] to convert the 614th amino acid from aspartic acid (D) to glycine (G) by overlap fusion PCR. The full-length infectious cDNA clone of SARS-CoV-2 D614G was assembled by *in vitro* ligation of seven contiguous cDNA fragments following the protocol previously described[10]. For construction of D614G mNeonGreen SARS-CoV-2, seven SARS-CoV-2 genome fragments (F1 to F5, F6 containing D614G mutation, and F7-mNG containing the mNeonGreen reporter gene) were prepared and *in vitro* ligated as described previously[10]. *In vitro* transcription was then preformed to synthesize full-length genomic RNA. For recovering the mutant viruses, the RNA transcripts were electroporated into Vero E6 cells. The viruses from electroporated cells were harvested at 40 h post electroporation and served as seed stocks for subsequent experiments. The D614G mutation from the recovered viruses was confirmed by sequence analysis. Viral titers were determined by plaque assay on Vero E6 cells. All virus preparation and experiments were performed in a biosafety level 3 (BSL-3) facilities. Viruses and plasmids are available from the World Reference Center for Emerging Viruses and Arboviruses at the University of Texas Medical Branch.

RNA extraction, RT-PCR, and Sanger sequencing.

Cell culture supernatants or clarified tissue homogenates were mixed with a five-fold excessof TRIzol™ LS Reagent (Thermo Fisher Scientific, Waltham, MA). Viral RNAs were extracted according to the manufacturer's instructions. The extracted RNAs were dissolved in 20 μl nuclease-free water. Two microliters of RNA samples were used for reverse transcription by using the SuperScript™ IV First-Strand Synthesis System (ThermoFisher Scientific) with random hexamer primers. Nine DNA fragments flanking the entire viral genome were amplified by PCR. The resulting DNAs were cleaned up by the QIAquick

PCR Purification Kit, and the genome sequences were determined by Sanger sequencing at GENEWIZ (South Plainfield, NJ).

The quantify viral RNA samples, quantitative real-time RT-PCR assays were performed using the iTaq SYBR Green One-Step Kit(Bio-Rad) on the LightCycler 480 system (Roche, Indianapolis, IN) following the manufacturers 'protocols. Primers are listed in Extended Data Table 1. The absolute quantification of viral RNA was determined by a standard curve method using an RNA standard (*in* vitrotranscribed3,839bp containing genomic nucleotide positions 26,044 to 29,883 of SARS-CoV-2 genome).

To quantify D614:G614 ratios for competition assays, a 663-bp RT-PCR product was amplified from extracted RNA using a SuperScript™ III One-Step RT-PCR kit (Invitrogen, Carlsbad, CA, USA). A 20-μl reaction was assembled in PCR 8-tube strips through the addition of 10μl 2× reaction mix, 0.4μlSuperScript III RT/Platinum Taq Mix, 0.8μlForward Primer (10 μM) (Extended Data Table 1), 0.8μl reverse primer (10 μM)(Extended Data Table 1), 4μl RNA, and 6μlRnase-free water. Reverse transcription and amplification was completed using the following protocol: (i) 55°C, 30 min; 94°C, 2 min; (ii) 94°C, 15s; 60°C, 30s; 68°C, 1min; 40 cycles; (iii) 68°C, 5 min; (iv) indefinite hold at 4°C. The presence and size of the desired amplicon was verified with 2μl of PCR product on an agarose gel. The remaining 18μl were purified by a QIAquick PCR Purification kit (Qiagen, Germantown, MD) according to the manufacturer's protocol.

Sequences of the purified RT-PCR products were generated using a BigDye Terminator v3.1 cycle sequencing kit (Applied Biosystems, Austin, TX, USA). The sequencing reactions were purified using a 96-well plate format (EdgeBio, San Jose, CA, USA) and analyzed on a 3500 Genetic Analyzer (Applied Biosystems, Foster City, CA). The peak electropherogram height representing each mutation site and the proportion of each competitor was analyzed using the QSVanalyser program[31].

Plaque assay.

Approximately 1.2×10^6 Vero E6 cells were seeded to each well of 6-well plates and cultured at 37°C, 5% CO_2 for 16 h. Virus was serially diluted in either DMEM with 2% FBS (for viral stocks and *in vitro*-generated samples) or DPBS (for hamster tissues) and 200μl was transferred to the monolayers. The viruses were incubated with the cells at 37°C with 5% $CO_2$for 1 h. After the incubation, overlay medium was added to the infected cells per well. The overlay medium contained either DMEM with 2% FBS and 1% sea-plaque agarose (Lonza, Walkersville, MD) in the case of *in vitro* samples or Opti-MEM with 2% FBS, 1% penicillin/streptomycin, and 0.8% agarose in the case of *in vivo* samples. After a 2-day incubation, plates were stained with neutral red (Sigma-Aldrich, St. Louis, MO) and plaques were counted on a light box.

Viral infection on cells.

Approximately 3×10^5Vero E6 or Calu-3 cells were seeded onto each well of 12-well plates and cultured at 37°C, 5% CO_2 for 16 h. Either SARS-CoV-2 D614 or G614 virus was inoculated into the cells at an MOI of 0.01. The virus was incubated with the cells at 37°C for 2 h. After the infection, the cells were washed by DPBS for 3 times to remove the un-

attached virus. One milliliter of culture medium was added into each well for the maintenance of the cells. At each time point, 100 μl of culture supernatants were harvested for the real-time qPCR detection and plaque assay. Meanwhile, 100μl fresh medium was added into each well to replenish the culture volume. The cells were infected in triplicates for each virus. All samples were stored in −80°C freezer until plaque or RT-PCR analysis.

Virion purification and spike protein cleavage analysis.

Vero E6 or Calu-3 2B4 cells were infected with D614 or G614 viruses at an MOI of 0.01. At 24 (for Vero)or 48 (Calu-3) hpi, the culture media were collected and clarified by low speed spin. Virions in the media were pelleted by ultracentrifugation through a 20% sucrose cushion at 26,000 rpm for 3 h at 4°C by in a BeckmanSW28 rotor. The purified virions were analyzed by Western blot using polyclonal antibodies against spike protein and nucleocapsid as described previously[32].

Viral infection in a primary human airway tissue model.

The EpiAirway system is a primary human airway 3D mucociliary tissue model consisting of normal, human-derived tracheal/bronchial epithelial (HAE) cells. For viral replication kinetics study, either D614 or G614 virus was inoculated onto the culture at an MOI of 5 in DPBS. After 2 h infection at 37°C with 5% CO_2, the inoculum was removed, and the culture was washed three times with DPBS. The infected epithelial cells were maintained without any medium in the apical well, and medium was provided to the culture through the basal well. The infected cells were incubated at 37°C, 5% CO_2. From day 1 to day 5, 300 μl DPBS were added onto the apical side of the airway culture and incubated at 37°C for 30 min to elute the released viruses. All virus samples in DPBS were stored at −80°C.

Hamster infection.

Four- to five-week-old male golden Syrian hamsters, strain HsdHan:AURA (Envigo, Indianapolis, IN), were inoculated intranasally with 2×10^4 PFU SARS-CoV-2 in a 100-μl volume. Eighteen animals received WT D614 virus, 18 received mutant G614 virus, and 18 received a mixture containing 10^4 PFU of D614virus and 10^4 PFU of G614 virus. The infected animals were weighed and monitored for signs of illness daily. On days 2, 4, and 7pi, cohorts of 6 infected animals and 4 (days 2 and 4) or 6 (day 7) mock-infected animals were anesthetized with isoflurane and nasal washes were collected in 400μl sterile DPBS. Animals were humanely euthanized immediately following the nasal wash. The trachea and the four lobes of the right lung were harvested in maintenance media (DMEM supplemented with 2% FBS and 1% penicillin/streptomycin) and stored at −80°C. Samples were subsequently thawed, tissues consisting of individual, intact lung lobes or the trachea were homogenized for 1 min at 26 sec-1, and debris was pelleted by centrifugation for 5 min at 16,100×g. Infectious titers were determined by plaque assay. Genomic RNAs were quantified by quantitative RT-PCR (Extended Data Table 1). Ratios of D614/G614RNA were determined via RT-PCR with quantification of Sanger peak heights.

Competition assay.

For the competition on primary human airway 3D tissue model, the D614 and G614 mutant viruses were mixed and inoculated onto the cells at a final MOI of 5. The initial ratio of D614 and G614 viruses is 1:1, 3:1, or 9:1based on PFU titers determined on Vero E6 cells. The DPBS with viruses was harvested every day from day 1 to 5 following the protocol described above. For the competition in hamsters, 100 μl mixtures of D614 and G614 viruses (total 2×10^4 PFU per hamster)were inoculated intranasally into 4–5 weeks old Syrian hamsters. On days2, 4, and 7 pi, 6 infected hamsters were sampled for competition detection. An aliquot of the inoculum for both hamster and human airway infections was backtitered for estimating the initial ratio of viruses. All samples were stored in −80°C freezer prior to analysis.

Validation of competition assay by Sanger sequencing.

To validate the consistency and accuracy of competition assay by Sanger sequencing, the D614/G614viruses were mixed at different ratios of 10:1, 5:1, 3:1, 1:1, 1:3, 1:5, 1:10 based on their PFU titers (total 10^6 PFU viruses) or mixed with10^6, 10^5, 10^4, 10^3,and 10^2 PFU of the two viruses at a ratio of 1:1. The total RNA of these mixed viruses was isolated and amplified by RT-PCR. The ratios of D614/G614 were calculated by the peak heights of Sanger sequencing. Data were analyzed by linear regression with correlation coefficients (r) and significance (p).

Stability assay of SARS-CoV-2.

Both D614 and G614 viruses were diluted to a final titer of 10^5 PFU/ml with DPBS. The diluted viruses were incubated in a 42°C, 37°C, or 33°C water bath. At indicated time points, 200 μl DPBS containing the viruses were taken out and stored in −80°C freezer. All the samples were then subjected to plaque assay on Vero E6 cells. The percentages of remaining infectious viruses were calculated by dividing the viral titers at each time point by the mean viral titer at 0 h.

Neutralization assay.

Neutralization assays were preformed using D614 and G614 mNeonGreen SARS-CoV-2 as previously described[21]. Briefly, Vero (CCL-81) cells were plated in black μCLEAR flat-bottom 96-well plate (Greiner Bio-one™). On the following day, sera or monoclonal antibodies were serially diluted from 1/20 starting dilution and nine 2-fold dilutions to the final dilution of 1/5,120 and incubated with D614 or G614 mNeonGreen SARS-CoV-2 at 37°C for 1 h. The virus-serum mixture was transferred to the Vero cell plate with the final MOI of 2.0. After 20 h, Hoechst 33342 Solution (400-fold diluted in Hank's Balanced Salt Solution; Gibco) was added to stain cell nucleus, sealed with Breath-Easy sealing membrane (Diversified Biotech), incubated at 37°C for 20 min, and quantified for mNeonGreen fluorescence using Cytation™ 7 (BioTek). The raw images (2×2 montage) were acquired using 4× objective, processed, and stitched using the default setting. The total cells (indicated by nucleus staining) and mNeonGreen-positive cells were quantified for each well. Infection rates were determined by dividing the mNeonGreen-positive cell number to total cell number. Relative infection rates were obtained by normalizing the infection rates of

serum-treated groups to those of non-serum-treated controls. The curves of the relative infection rates versus the serum dilutions (log10 values) were plotted using Prism 8 (GraphPad). A nonlinear regression method was used to determine the dilution fold that neutralized 50% of mNeonGreen fluorescence (NT_{50}). Each serum was tested in duplicates.

Statistics.

Male hamsters were randomly allocated into different groups. The investigators were not blinded to allocation during the experiments or to the outcome assessment. *A priori* power analysis for two independent groups having a 1.0log_{10} titer difference with a standard deviation of 0.5log_{10}, assuming an alpha of 0.05 and a power of 0.8 with a two-tailed t-test, dictated that animal experiments include n=6 subjects per cohort. Descriptive statistics have been provided in the figure legends. For *in vitro* replication kinetics, Kruskal–Wallis analysis of variance was conducted to detect any significant variation among replicates. If no significant variation was detected, the results were pooled for further comparison. Differences between continuous variables were assessed with a non-parametric Mann–Whitney test. Hamster weights were analyzed by two factor ANOVA, with the percent weight change as the dependent variable and the strain and time as fixed factors. Tukey's post-hoc test was used to compare all cohort pairs on days 1–7 pi. Log_{10}-tranformed titers were analyzed by two-factor repeated measures ANOVA with the organ and strain as fixed factors. Sidak's post-hoc test was used to compare strains within each organ. Genomic RNA/PFU ratios were calculated from non-transformed values, and the resulting ratios were log_{10}-transformed prior to two factor repeated measures ANOVA with the organ and strain as fixed factors and Sidak's post-hoc test to compare strains within a given organ. When a sample was below the limit of detection, it was treated as half of the limit of detection value for statistical and graphing purposes. Analysis was performed in Prism version 7.03 (GraphPad, San Diego, CA).

For virus competition experiments, relative replicative fitness values for G614 strain over D614 strain were analyzed according to w=(f0/i0), where i0 is the initial D614/G614 ratio and f0 is the final D614/G614 ratio after competition. Sanger sequencing (initial timepoint T0) counts for each virus strain being compared were based upon average counts over three replicate samples of inocula per experiment, and post-infection (timepoint T1) counts were taken from samples of individual subjects. For the primary human airway samples, multiple experiments were performed, so that f0/i0 was clustered by experiment. To model f0/i0, the ratio T0/T1 was found separately for each subject in each strain group, log (base-10) transformed to an improved approximation of normality, and modeled by analysis of variance with relation to group, adjusting by experiment when appropriate to control for clustering within experiment. Specifically, the model was of the form Log10_CountT1overCountT0 ~ Experiment + Group. Fitness ratios between the two groups [the model's estimate of w=(f0/i0)] were assessed per the coefficient of the model's Group term, which was transformed to the original scale as 10êoefficient. This modeling approach compensates for any correlation due to clustering within experiment similarly to that of corresponding mixed effect models, and is effective since the number of experiments was small. Statistical analyses were performed using R statistical software (R Core Team, 2019, version 3.6.1). In all statistical tests, two-sided alpha=.05. Catseye plots[33], which illustrate

the normal distribution of the model-adjusted means, were produced using the “catseyes” package[34].

Extended Data

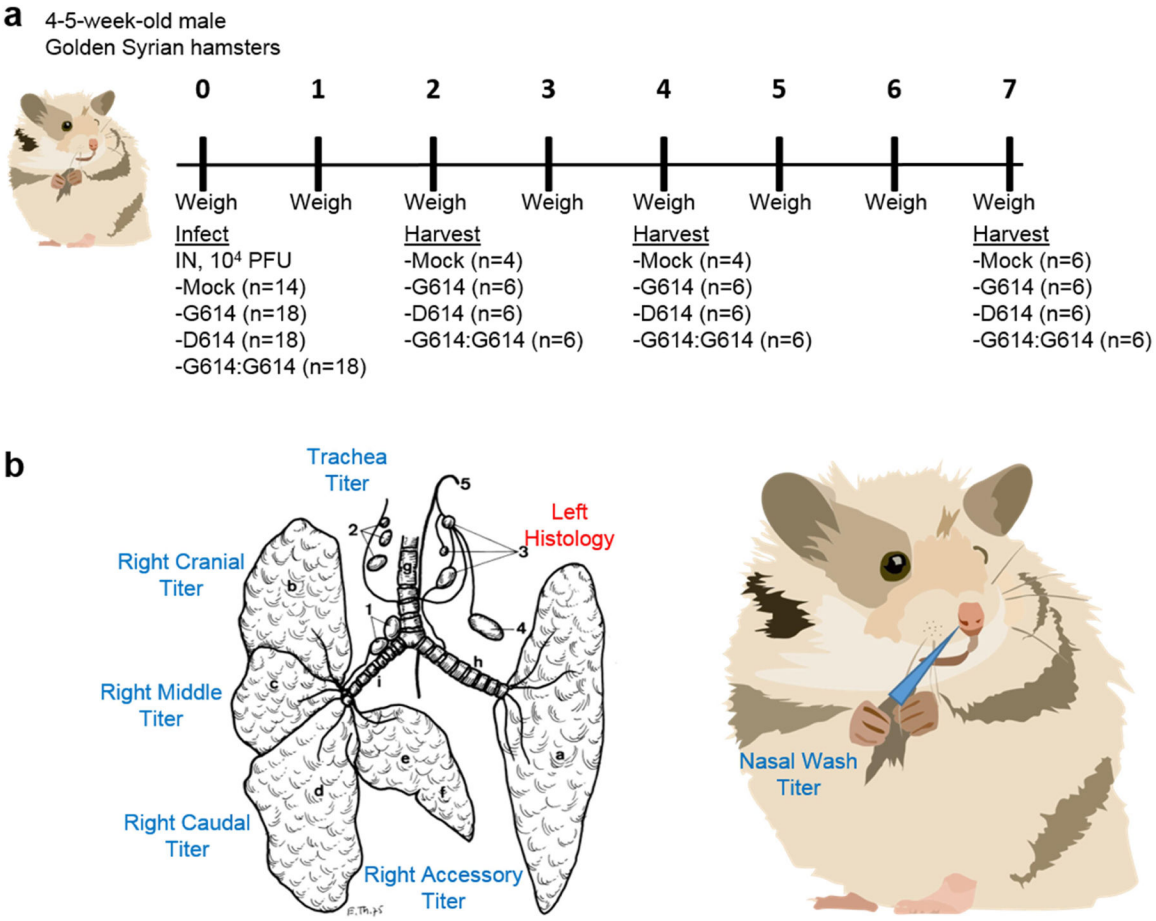

Extended Data Figure 1. Experimental design of hamster infection and sample harvest.

(a) Graphical overview of experiment to assess the impact of G614 mutation on replication in the respiratory system of hamsters. **(b)** Schematic organs harvested from hamsters sacrificed on days 2, 4, and 7 post-infection. Illustration of hamster lung adapted from Reznik, G. *et al. Clinical anatomy of the European hamster. Cricetuscricetus, L.*, For sale by the Supt of Docs, U.S. Govt. Print. Off., 1978.

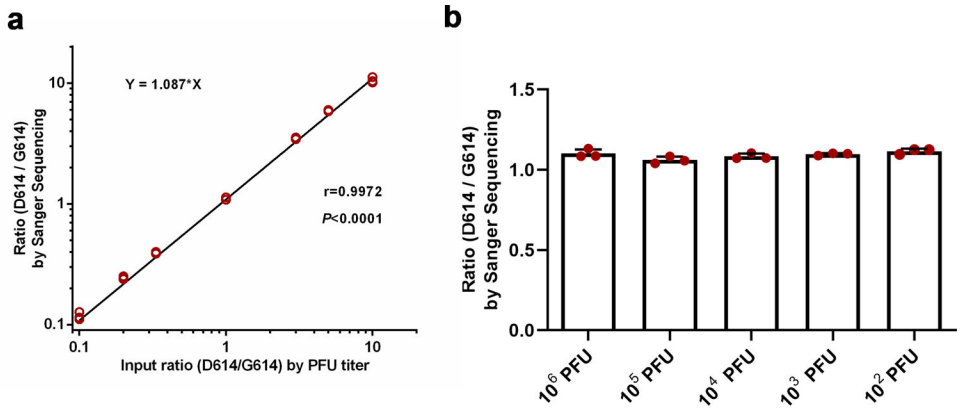

Extended Data Figure 2. Validation of competition assay by Sanger sequencing.

(a) The correlation between input PFU ratios and output RT-PCR amplicon ratios determined by Sanger sequencing. D614 and G614 viruses were mixed at PFU ratios of 10:1, 5:1, 3:1, 1:1, 1:3, 1:5, or 1:10. Total RNA of the virus mixtures were extracted and amplified by RT-PCR. The D614/G614 ratios were calculated by the peak heights of Sanger sequencing. Data were analyzed by linear regression with correlation coefficients (r) and significance (p). Symbols represent individual replicates and the solid line represents the fitted line. Data is derived from a single experiment conducted in duplicate. **(b)** Assay range evaluation. The ratio of D614/G614virus mixture calculated from Sanger sequencing was consistent when using a wide range of virus amounts. The D614/G614 viruses were mixed at 1:1PFU ratio. The total titers of the mixed viruses were 10^2, 10^3, 10^4, 10^5, and 10^6 PFU. The total RNA of virus mixture was isolated and amplified by RT-PCR. The D614/G614 ratios were calculated by the peak heights from Sanger sequencing. Symbols represent individual replicates, bar heights represent the mean, and error bars represent the standard deviation. Data is derived from a single experiment conducted in triplicate.

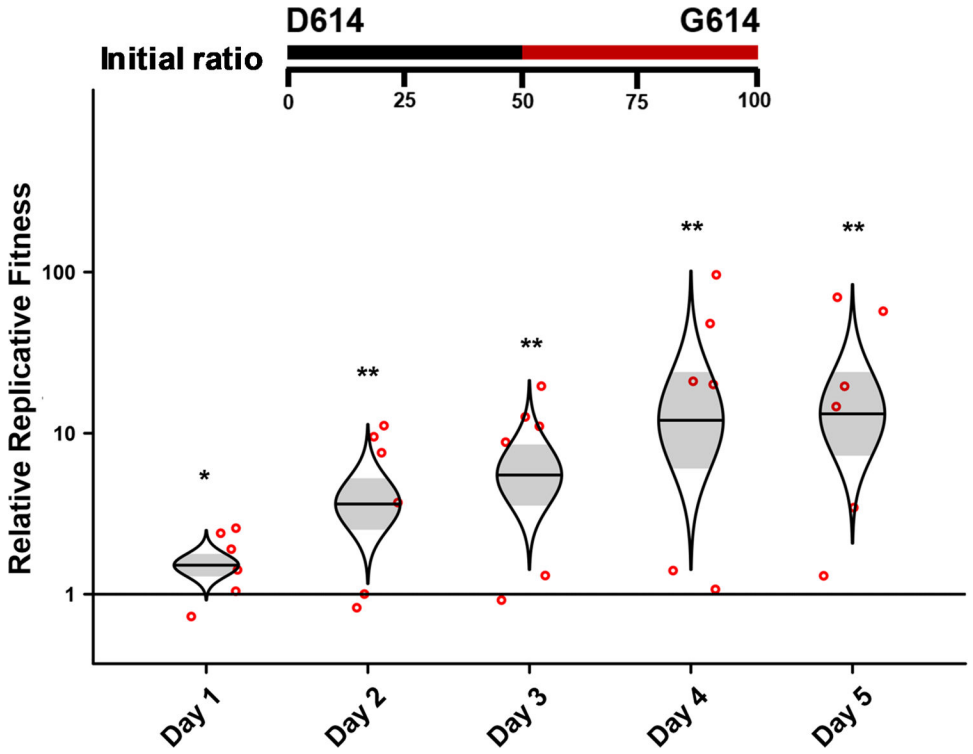

Extended Data Figure 3. D614G substitution significantly enhances SARS-CoV-2 replication in primary human airway tissues from a different donor.

D614 and G614 viruses were equally mixed and inoculated onto the airway tissue at a total MOI of 5. This airway tissue was produced from a different donor than that used in Figure 3. The tissues were washed by DPBS to collect the secreted viruses every day from days 1 to 5. The total RNAs were isolated and amplified by RT-PCR. The ratio of D614 and G614 viruses after competition were measure by Sanger sequencing. Circles represent individual samples (n=6, two independent experiments conducted in triplicate). The midline represents the sample mean, and the shaded region represents +/− one unit of standard error about the mean. The width of the catseye plot represents the distribution of the model-adjusted means, and the heights extend to span 99.8% of the distribution of the mean. The y-axis is displayed on the $\log_{10}$ scale such that the null value is 1. P values are calculated for the group (strain) coefficient for each linear regression model, and are reported for all instances of $p<0.05$.

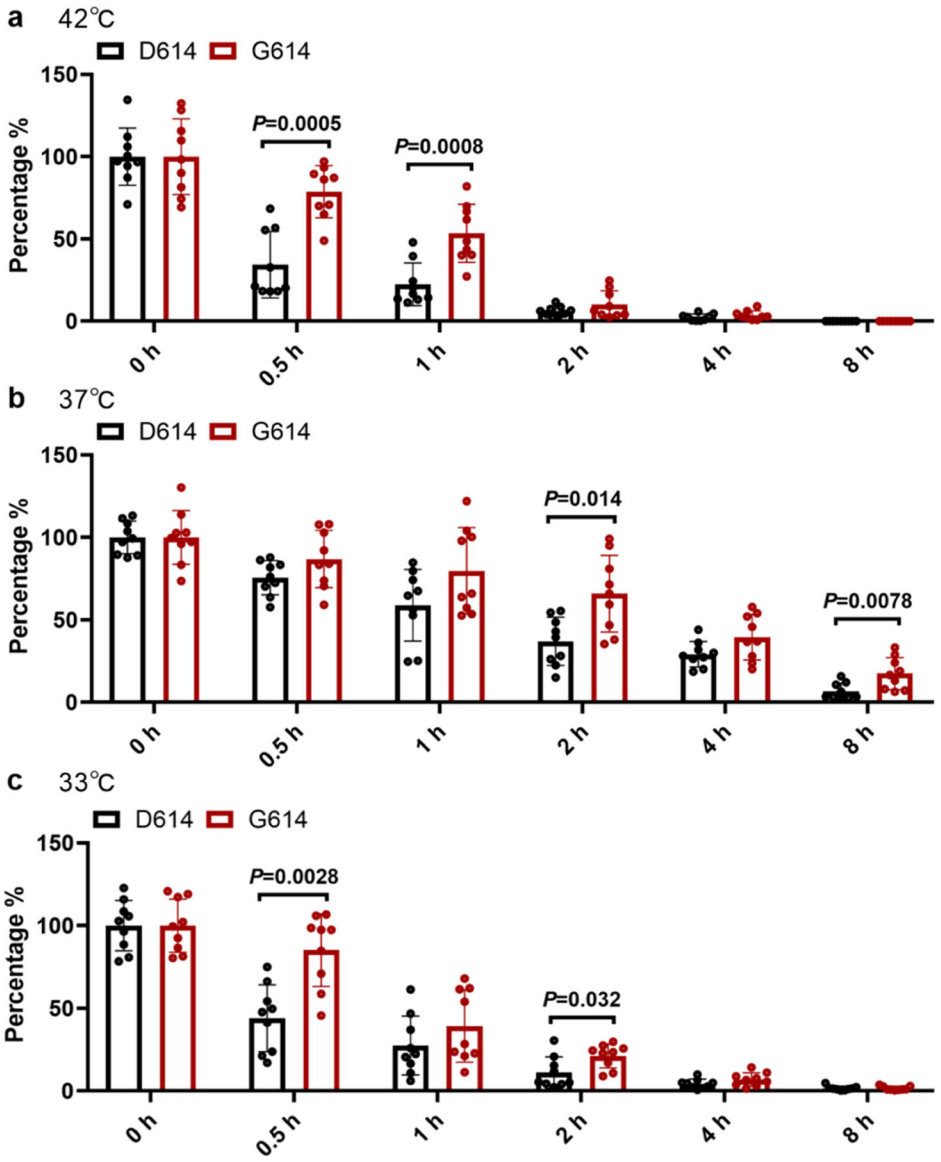

Extended Data Figure 4. SARS-CoV-2 G614 is more stable than D614.

Equal amounts (10^5 PFU/ml) of D614 and G614 viruses were incubated in DPBS at 42°C (**a**), at 37°C (**b**), or 33°C (**c**), respectively. At 0 h, 0.5 h, 1 h, 2 h, 4 h, and 8 h, the viruses were quantified for their infectious levels by plaque assay on Vero E6 cells. The detect limitation of plaque assay is 10 PFU/ml. The percentage of remaining infectious viruses were normalized by the average titers at 0 h. Symbols represent individual replicates, bar heights represent the mean, and error bars represent the standard deviation. *P* values were determined by two-tailed Mann-Whitney test (n=9, from three independent experiments, each conducted in triplicate), and results of $p<0.05$ are indicated.

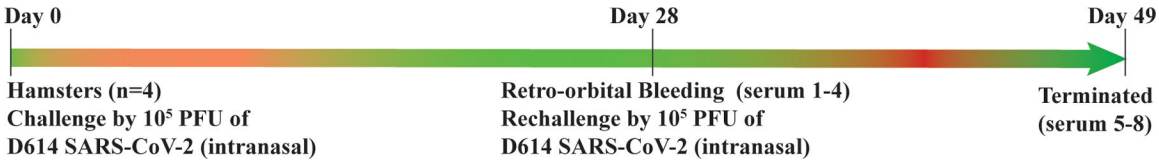

Extended Data Figure 5. Scheme for preparing the D614 SARS-CoV-2-infected hamster sera for neutralization assay.

Eight sera were collected: Four sera (number 1–4) collected on day 28 post infection and another four sera (number 5–8) collected on day 49 after the second viral infection.

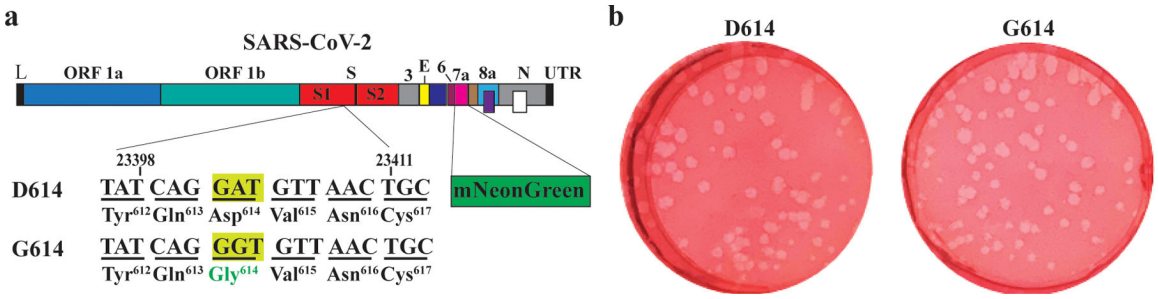

Extended Data Figure 6. Construction of G614 mNeonGreen SARS-CoV-2.

(a) Diagram of the construction. The D614G mutation was introduced into a mNeonGreen reporter SARS-CoV-2 using the method as described previously[10]. **(b)** Plaque morphologies of D614 and G614 mNeonGreen SARS-CoV-2.

a

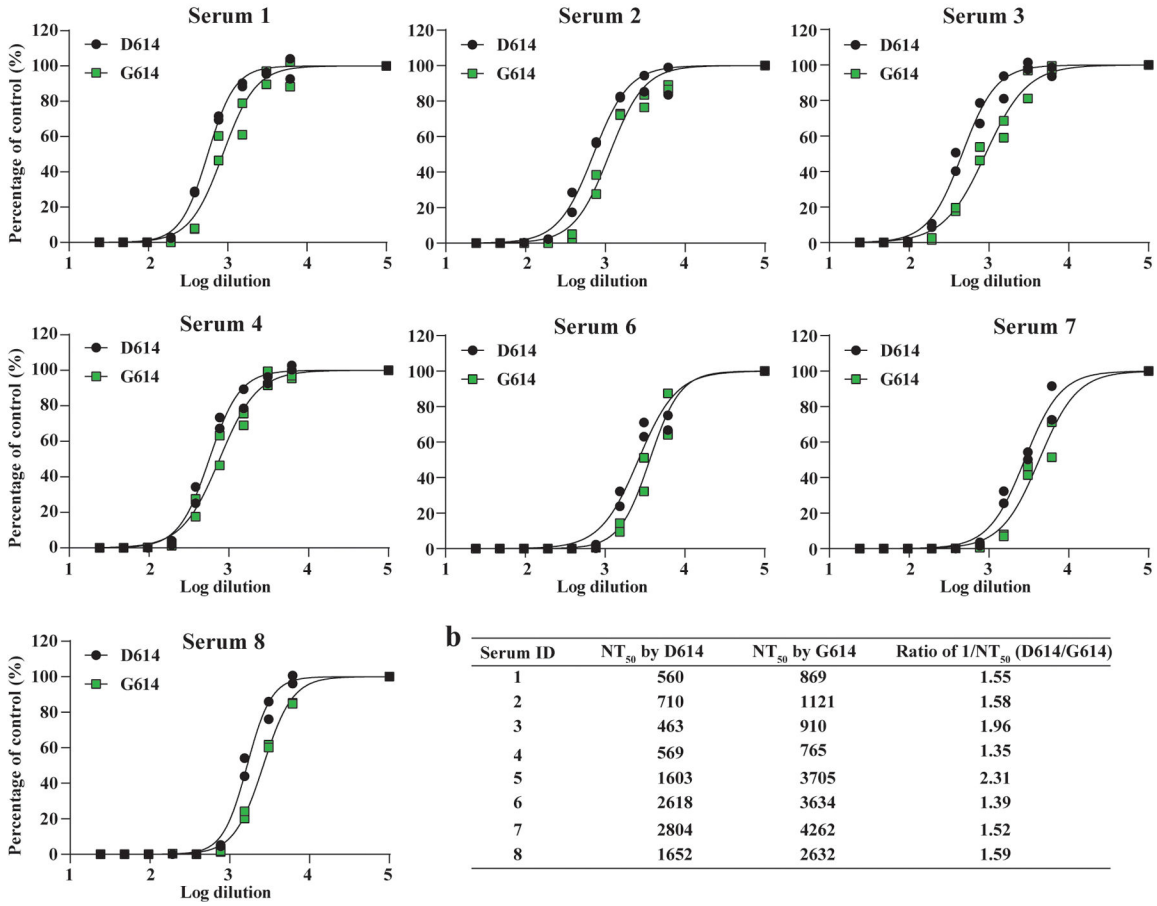

b

Serum ID	NT_{50} by D614	NT_{50} by G614	Ratio of $1/NT_{50}$ (D614/G614)
1	560	869	1.55
2	710	1121	1.58
3	463	910	1.96
4	569	765	1.35
5	1603	3705	2.31
6	2618	3634	1.39
7	2804	4262	1.52
8	1652	2632	1.59

Extended Data Figure 7. Neutralization activities of hamster sera against D614 and G614 mNeonGreen SARS-CoV-2.

(a) Neutralizing curves of eight hamster sera against D614 and G614 mNeonGreenSARS-CoV-2. The neutralizing curve for serum 5 is shown in Fig. 4c. Symbols represent individual samples and the solid line represents the fitted curve. Data is derived from a single experiment conducted in duplicate. **(b)** Calculated NT_{50} values and ratios of $1/NT_{50}$ for all eight hamster sera. The mean ratios were determined by (D614 $1/NT_{50}$)/(G614 $1/NT_{50}$).

a

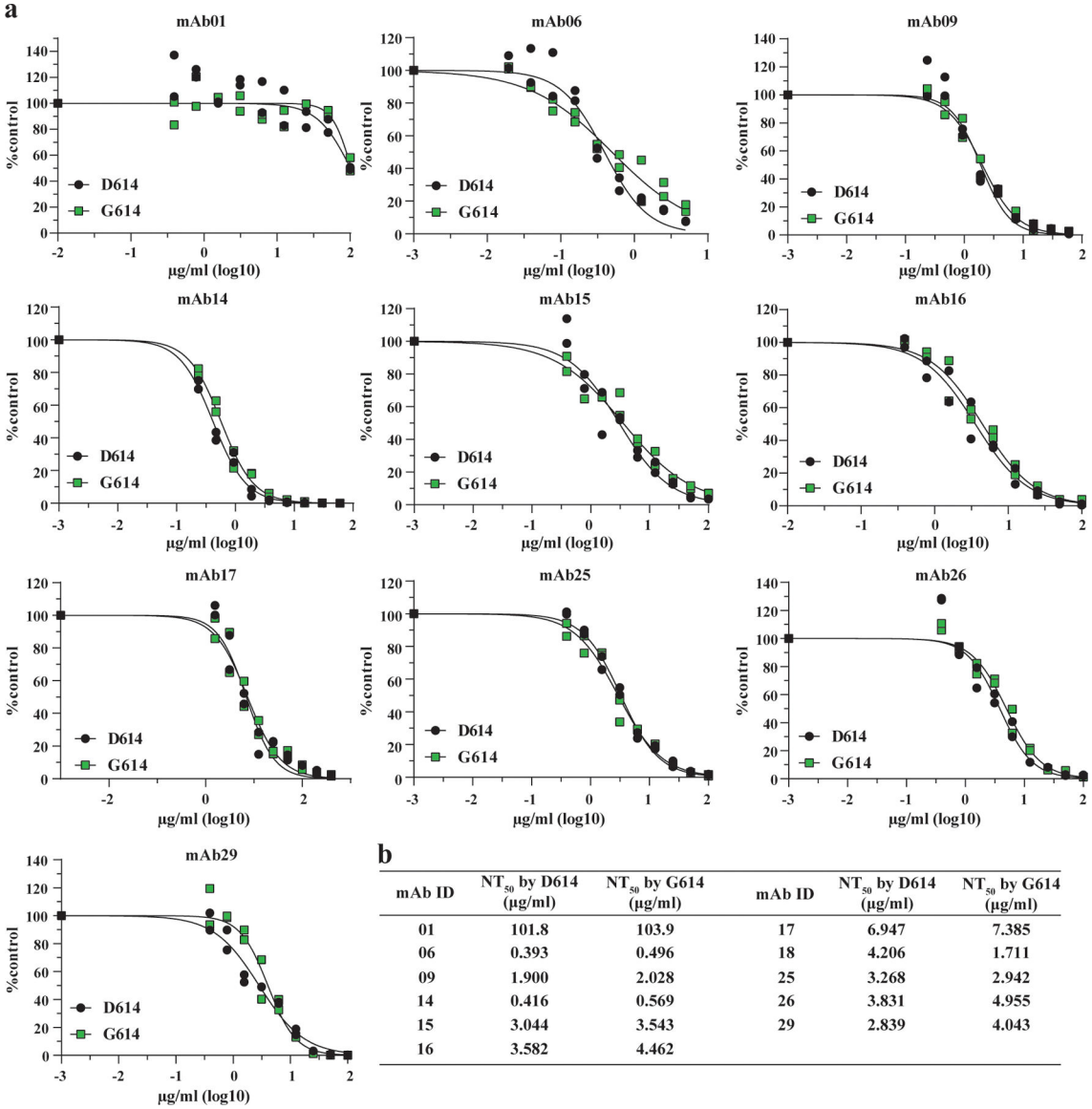

b

mAb ID	NT_{50} by D614 (µg/ml)	NT_{50} by G614 (µg/ml)	mAb ID	NT_{50} by D614 (µg/ml)	NT_{50} by G614 (µg/ml)
01	101.8	103.9	17	6.947	7.385
06	0.393	0.496	18	4.206	1.711
09	1.900	2.028	25	3.268	2.942
14	0.416	0.569	26	3.831	4.955
15	3.044	3.543	29	2.839	4.043
16	3.582	4.462			

Extended Data Figure 8. Neutralization activities of human mAbs against D614 and G614 mNeonGreen SARS-CoV-2 in Experiment I.

(a) Neutralizing curves of eleven mAbs against D614 and G614 reporter SARS-CoV-2. The neutralizing curve for mAb18 is shown in Fig. 4f. Symbols represent individual replicates and the solid line represents the fitted curve. Data is derived from a single experiment conducted in duplicate. **(b)** Calculated NT_{50} values for all eleven mAbs.

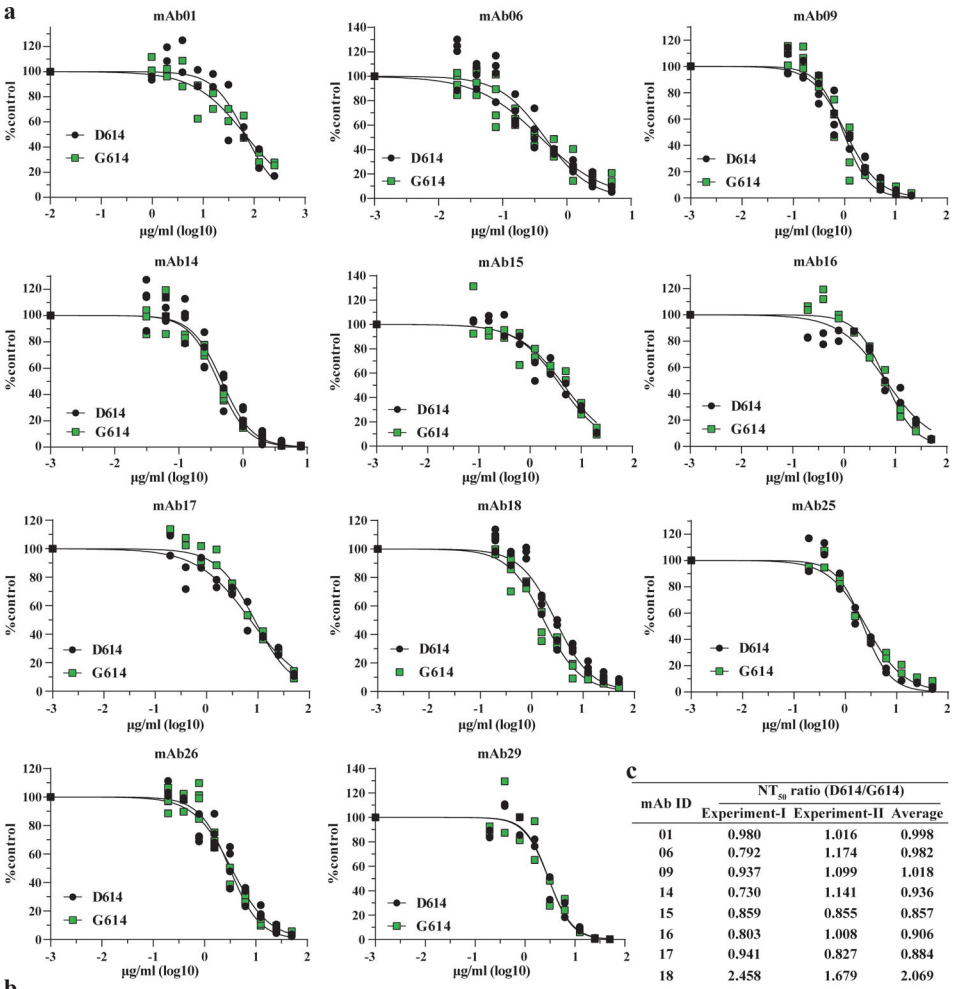

b

mAb ID	NT_{50} by D614 (µg/ml)	NT_{50} by G614 (µg/ml)	mAb ID	NT_{50} by D614 (µg/ml)	NT_{50} by G614 (µg/ml)
01	67.25	66.16	17	7.119	8.610
06	0.452	0.385	18	2.892	1.722
09	1.037	0.943	25	2.261	2.550
14	0.469	0.411	26	3.337	3.075
15	3.929	4.597	29	2.969	2.956
16	6.465	6.412			

c

mAb ID	NT_{50} ratio (D614/G614)		
	Experiment-I	Experiment-II	Average
01	0.980	1.016	0.998
06	0.792	1.174	0.982
09	0.937	1.099	1.018
14	0.730	1.141	0.936
15	0.859	0.855	0.857
16	0.803	1.008	0.906
17	0.941	0.827	0.884
18	2.458	1.679	2.069
25	1.110	0.887	0.999
26	0.773	0.760	0.767
29	0.702	1.004	0.853

Extended Data Figure 9. Neutralization activities of human mAbs against D614 and G614 mNeonGreen SARS-CoV-2 in Experiment II.

(a) Neutralizing curves of eleven mAbs against D614 and G614 reporter SARS-CoV-2. Symbols represent individual replicates and the solid line represents the fitted curve. Data is derived from a single experiment conducted in either duplicate or quadruplicate. **(b)** Calculated NT_{50} values for all eleven mAbs. (c) Summary of NT_{50} ratios from two independent experiments. The ratios were determined by (D614 NT_{50})/(G614 NT_{50})

Extended Data Table 1.
Primers for gene cloning and qPCR.

Primer sequences for the generation of the D614G mutation, as well as for the detection, sequencing, and quantification of SARS-CoV-2 are reported.

Primers for cloning SARS-CoV-2 G614 mutant	**Forward primer**	**Reverse primer**
SARS-CoV-2 S-D614G Fragment 1	*CATTTGTGGGTTTATACAACAAAAG*	*TGTGCAGTTAACAcCCTGATAAAGAACAGC*
SARS-CoV-2 S-D614G Fragment 2	*GCTGTTCTTTATCAGGgTGTTAACTGCACA*	*CTGGATTGAATGACCACATGGAAC*
SARS-CoV-2 S-D614G overlap PCR	*CAATCAAGCCAGCTATAAAACC*	*CTGGATTGAATGACCACATGGAAC*
Primers for one-step RT-PCR	**Forward primer**	**Reverse primer**
SARS-CoV-2 22685F-23865R	*AGGCACAGGTGTTCTTAC*	*GTTAAAGCACGGTTTAATTGTG*
Primers for sanger sequencing	**Forward primer**	
SARS-CoV-2 22685F	*AGGCACAGGTGTTCTTAC*	
The primers for SBR RT-qPCR	**Forward primer**	**Reverse primer**
SARS-CoV-2 ORF 8	*AATCAGCACCTTTAATTGAATTG*	*CAGGAAACTGTATAATTACCGATA*

Supplementary Material

Refer to Web version on PubMed Central for supplementary material.

Acknowledgments

This research was supported by grants from NIA and NIAID of the NIH [AI153602 and AG049042 to V.D.M.; R24AI120942 (WRCEVA) to S.C.W] and by STARs Award provided by the University of Texas System to V.D.M. X.X. was partially supported by NIH5UC7AI094660.P.-Y.S. was supported by NIH grants AI142759, AI134907, AI145617, and UL1TR001439, and awards from the Sealy & Smith Foundation, Kleberg Foundation, the John S. Dunn Foundation, the Amon G. Carter Foundation, the Gilson Longenbaugh Foundation, and the Summerfield Robert Foundation. A.M. is supported by a Clinical and Translational Science Award NRSA (TL1) Training Core (TL1TR001440) from NIH.J.L. and C.R.F.-G. were supported by the McLaughlin Fellowship at the University of Texas Medical Branch.

Data Availability Statement.

Data associated with all figures may be accessed via the Figshare data repository at doi:10.6084/m9.figshare.13030430.

References

1. Korber B et al. Tracking Changes in SARS-CoV-2 Spike: Evidence that D614G Increases Infectivity of the COVID-19 Virus. Cell, 10.1016/j.cell.2020.06.043 (2020).
2. Yurkovetskiy L et al. Structural and Functional Analysis of the D614G SARS-CoV-2 Spike Protein Variant. BioRxiv (2020).
3. Zhou P et al. A pneumonia outbreak associated with a new coronavirus of probable bat origin. Nature 579, 270–273, 10.1038/s41586-020-2012-7 (2020). [PubMed: 32015507]
4. Domingo P et al. The four horsemen of a viral Apocalypse: The pathogenesis of SARS-CoV-2 infection (COVID-19). EBioMedicine 58, 102887, 10.1016/j.ebiom.2020.102887 (2020). [PubMed: 32736307]
5. Smith EC, Blanc H, Surdel MC, Vignuzzi M & Denison MR Coronaviruses lacking exoribonuclease activity are susceptible to lethal mutagenesis: evidence for proofreading and potential therapeutics. PLoS Pathog 9, e1003565, 10.1371/journal.ppat.1003565 (2013). [PubMed: 23966862]
6. Fauver JR et al. Coast-to-Coast Spread of SARS-CoV-2 during the Early Epidemic in the United States. Cell 181, 990–996 e995, 10.1016/j.cell.2020.04.021 (2020). [PubMed: 32386545]
7. Song HD et al. Cross-host evolution of severe acute respiratory syndrome coronavirus in palm civet and human. Proc Natl Acad Sci U S A 102, 2430–2435, 10.1073/pnas.0409608102 (2005). [PubMed: 15695582]
8. Hou YJ et al. SARS-CoV-2 Reverse Genetics Reveals a Variable Infection Gradient in the Respiratory Tract. Cell 182, 1–18 (2020). [PubMed: 32649872]
9. Lorenzo-Redondo R et al. A Unique Clade of SARS-CoV-2 Viruses is Associated with Lower Viral Loads in Patient Upper Airways. medRxiv, 10.1101/2020.05.19.20107144 (2020).
10. Xie X et al. An Infectious cDNA Clone of SARS-CoV-2. Cell Host Microbe 27, 841–848 e843, 10.1016/j.chom.2020.04.004 (2020). [PubMed: 32289263]
11. Harcourt J et al. Severe Acute Respiratory Syndrome Coronavirus 2 from Patient with 2019 Novel Coronavirus Disease, United States. Emerg Infect Dis 26, 10.3201/eid2606.200516 (2020).
12. Chan JF et al. Simulation of the clinical and pathological manifestations of Coronavirus Disease 2019 (COVID-19) in golden Syrian hamster model: implications for disease pathogenesis and transmissibility. Clin Infect Dis, 10.1093/cid/ciaa325 (2020).
13. Wiser MJ & Lenski RE A Comparison of Methods to Measure Fitness in Escherichia coli. PLoS One 10, e0126210, 10.1371/journal.pone.0126210 (2015). [PubMed: 25961572]
14. Grubaugh ND et al. Genetic Drift during Systemic Arbovirus Infection of Mosquito Vectors Leads to Decreased Relative Fitness during Host Switching. Cell Host Microbe 19, 481–492, 10.1016/j.chom.2016.03.002 (2016). [PubMed: 27049584]
15. Bergren NA et al. “Submergence” of Western equine encephalitis virus: Evidence of positive selection argues against genetic drift and fitness reductions. PLoS Pathog 16, e1008102, 10.1371/journal.ppat.1008102 (2020). [PubMed: 32027727]
16. Coffey LL & Vignuzzi M Host alternation of chikungunya virus increases fitness while restricting population diversity and adaptability to novel selective pressures. J Virol 85, 1025–1035, 10.1128/JVI.01918-10 (2011). [PubMed: 21047966]
17. Bai J et al. Phenotypic responses of differentiated asthmatic human airway epithelial cultures to rhinovirus. PLoS One 10, e0118286, 10.1371/journal.pone.0118286 (2015). [PubMed: 25706956]
18. Jackson GR Jr., Maione AG, Klausner M & Hayden PJ Prevalidation of an Acute Inhalation Toxicity Test Using the EpiAirway In Vitro Human Airway Model. Appl In Vitro Toxicol 4, 149–158, 10.1089/aivt.2018.0004 (2018).
19. Mulligan MJ et al. Phase 1/2 study of COVID-19 RNA vaccine BNT162b1 in adults. Nature, 10.1038/s41586-020-2639-4 (2020).
20. Jackson LA et al. An mRNA Vaccine against SARS-CoV-2 - Preliminary Report. N Engl J Med, 10.1056/NEJMoa2022483 (2020).
21. Muruato AE et al. A high-throughput neutralizing antibody assay for COVID-19 diagnosis and vaccine evaluation. Nature Communications, In press, 10.1101/2020.05.21.109546 (2020).

22. Hoffmann M et al. SARS-CoV-2 Cell Entry Depends on ACE2 and TMPRSS2 and Is Blocked by a Clinically Proven Protease Inhibitor. Cell 181, 271–280 10.1016/j.cell.2020.02.052 (2020). [PubMed: 32142651]
23. Hoffmann M, Kleine-Weber H & Pohlmann S A Multibasic Cleavage Site in the Spike Protein of SARS-CoV-2 Is Essential for Infection of Human Lung Cells. Mol Cell 78, 779–784 e775, 10.1016/j.molcel.2020.04.022 (2020). [PubMed: 32362314]
24. Zhang L et al. The D614G mutation in the SARS-CoV-2 spike protein reduces S1 shedding and increases infectivity. bioRxiv, 10.1101/2020.06.12.148726 (2020).
25. Daniloski Z, Guo X & Sanjana NE The D614G mutation in SARS-CoV-2 Spike increases transduction of multiple human cell types. bioRxiv, 10.1101/2020.06.14.151357 (2020).
26. Wolfel R et al. Virological assessment of hospitalized patients with COVID-2019. Nature 581, 465–469, 10.1038/s41586-020-2196-x (2020). [PubMed: 32235945]
27. Sungnak W et al. SARS-CoV-2 entry factors are highly expressed in nasal epithelial cells together with innate immune genes. Nat Med 26, 681–687, 10.1038/s41591-020-0868-6 (2020). [PubMed: 32327758]
28. Wagner C et al. Comparing viral load and clinical outcomes in Washington State across D614G substitution in spike protein of SARS-CoV-2, <https://github.com/blab/ncov-wa-d614g> (2020).
29. Hou Yixuan J, Peter Halfmann SC, Ehre Camille, Kuroda Makoto, Dinnon Kenneth H III, Leist Sarah R, Schäfer Alexandra, Nakajima Noriko, Takahashi Kenta, Lee Rhianna E, Mascenik Teresa M, Edwards Caitlin E, Tse Longping V, Boucher Richard C, Randell Scott H, Suzuki Tadaki, Gralinski Lisa E, Kawaoka Yoshihiro, Baric Ralph S. SARS-CoV-2 D614G Variant Exhibits Enhanced Replication ex vivo and Earlier Transmission in vivo. BioRxiv, 10.1101/2020.1109.1128.317685.
30. Richard M et al. Influenza A viruses are transmitted via the air from the nasal respiratory epithelium of ferrets. Nat Commun 11, 766, 10.1038/s41467-020-14626-0 (2020). [PubMed: 32034144]

References Specific to the Methods Section

31. Carr IM et al. Inferring relative proportions of DNA variants from sequencing electropherograms. Bioinformatics 25, 3244–3250, 10.1093/bioinformatics/btp583 (2009). [PubMed: 19819885]
32. Johnson BA et al. Furin Cleavage Site Is Key to SARS-CoV-2 Pathogenesis. bioRxiv, 10.1101/2020.1108.1126.268854 (2020).
33. Cumming G The New Statistics: Why and How. Psychol. Sci, 7–29, 10.1177/0956797613504966 (2014). [PubMed: 24220629]
34. Andersen C Catseyes: Create Catseye Plots Illustrating the Normal Distribution of the Means. R package version 0.2.3 (2019).

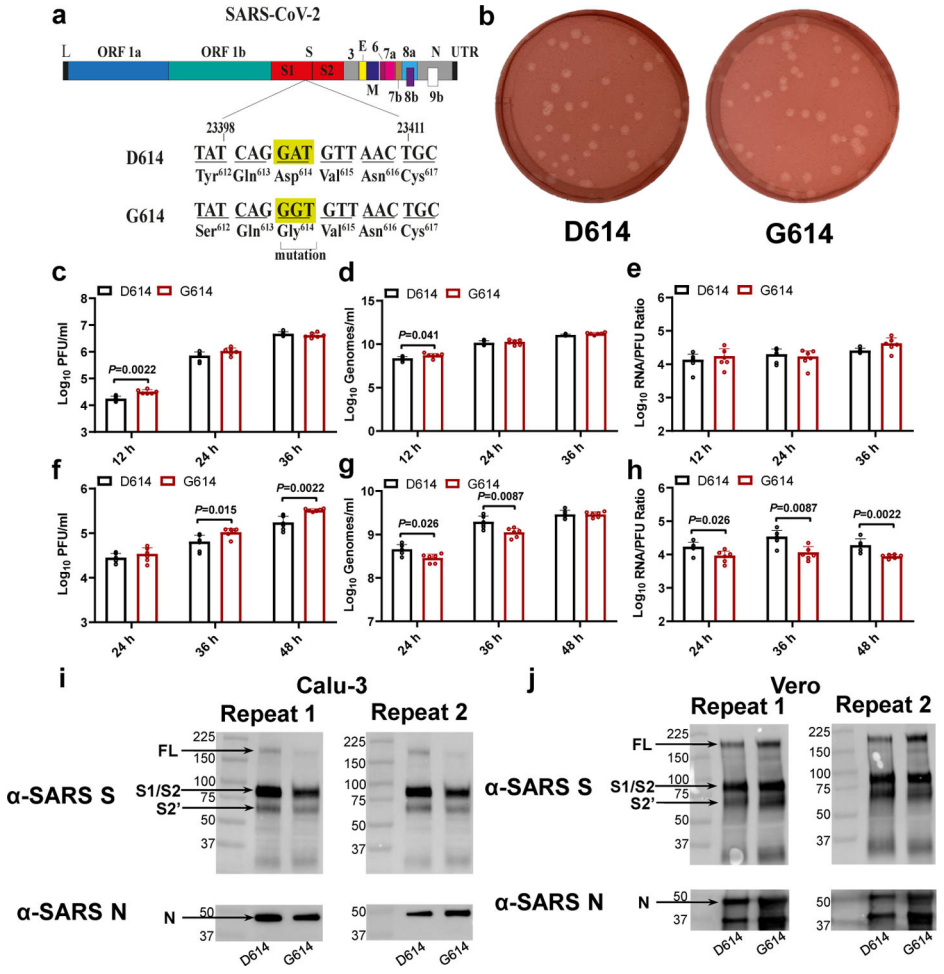

Figure 1. D614G substitution improves SARS-CoV-2 replication on Calu-3 cells through increased virion infectivity.

(a) Construction of mutant G614 SARS-CoV-2. A single nucleotide A-to-G substitution was introduced to construct the spike D614G mutation in the infectious cDNA clone of SARS-CoV-2. **(b)** Plaque morphologies of D614 and G614 viruses, developed on day 2 pi in Vero E6 cells. **(c-h)** Viral replication and genomic RNA/PFU ratios of D614 and G614 viruses produced from Vero E6 cells (c-e) and from Calu-3 cells (f-h). Cells were infected at an MOI of 0.01. Infectious viral titers (c,f) and genomic RNA levels (d,g) in culture medium were determined by plaque assay and real-time RT-qPCR, respectively. The genomic RNA/PFU ratios (e,h) were calculated to indicate virion infectivity. Symbols represent individual samples, bar heights represent means, and error bars represent standard deviations. *P* values were determined by two-tailed Mann–Whitney test from a sample size of n=6 (two independent experiments, conducted in triplicate). All results of $p<0.05$ are reported. **(i,j)** Spike protein cleavage of purified virions. Purified D614 and G614 virions were analyzed by Western blot using polyclonal antibodies against spike and nucleocapsid. Full-length spike [20], S1/S2 cleavage form, and S2' protein are annotated. Results from two independent experiments are presented for virions produced from Calu-3 cells (i) and Vero E6 cells (j).

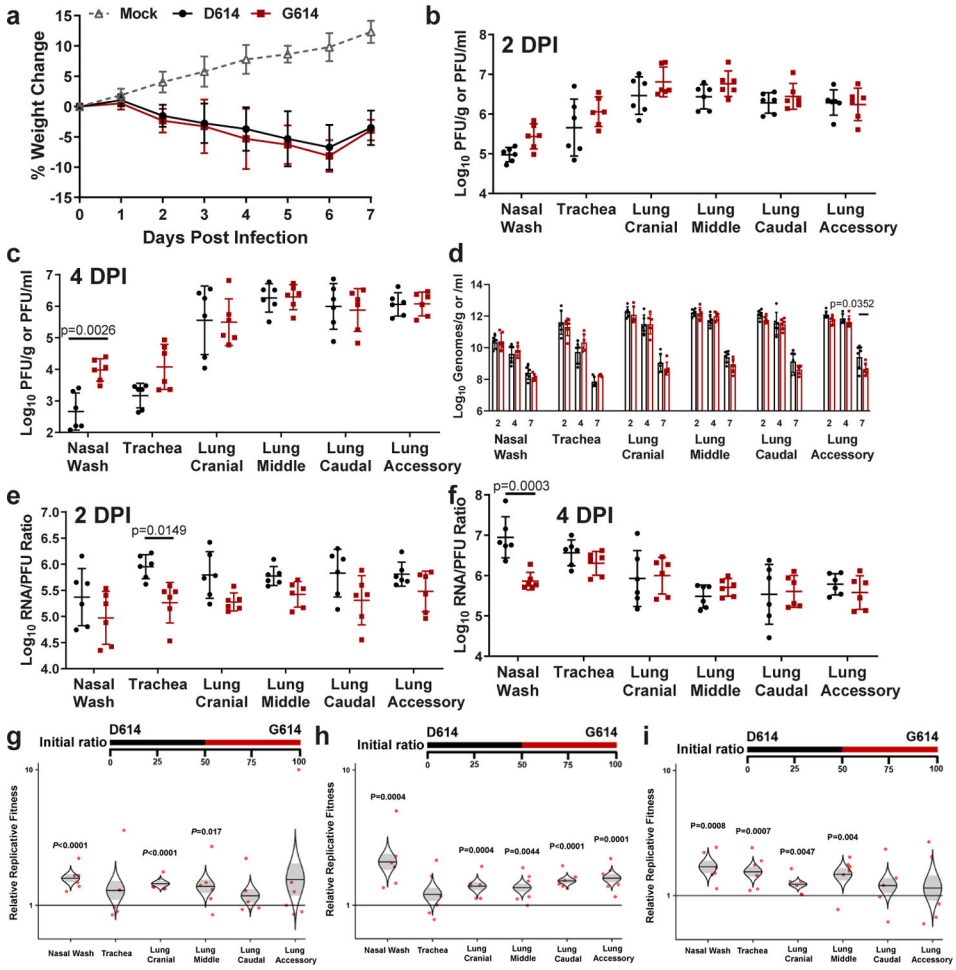

Figure 2. D614G substitution increases SARS-CoV-2 replication in the upper airway, but not the lungs, of hamsters.

(a-i) 3–4-Week-old male golden Syrian hamsters were infected intranasally with 2×10^4 PFU of D614 or G614 SARS-CoV-2, or PBS. All data are from a single experiment. (a) Weight loss was monitored for seven days pi. Symbols represent means, error bars represent standard deviation. Sample sizes were n=18 for infected cohorts and n=14 for the mock cohort at days 0–2, n=12 for infected cohorts and n=10 for the mock cohort at days 3–4, and n=6 for all cohorts at days 5–7. Weight loss was analyzed by two-factor ANOVA with Tukey's post-hoc test, with $p>0.05$ at all timepoints. (b,c) Infectious titers and (d) viral genomes were measured in the nasal wash, trachea, and lung on days 2 (b,d), 4 (c,d), and 7 (d) pi. (e,f) Genome/PFU ratios on days 2 (e) and 4 (f) pi were calculated as a measure of infectivity. (b-f) Symbols represent individual animals (n=6). Midlines (b,c,e,f) and bar heights (d) represent means. (b-f) Error bars represent standard deviation. Two-factor ANOVA with Sidak's post-hoc test are reported for $p<0.05$. **(g-i)** Hamsters were inoculated with 1:1 mixtures of D614 and G614 viruses (10^4 PFU each). Nasal wash, trachea, and lung were collected on days 2 (g), 4 (h), and 7 (i) pi. Relative fitness was assessed by Sanger sequencing. (g-i) Circles represent individual animals (n=6). Midline represents the mean. Shaded regions represent one unit of standard error about the mean. The width of the catseye plot represents the distribution of the model-adjusted means, and heights extend to 99.8% of

the distribution. The y-axis is $\log_{10}$ scaled. P values are calculated for the group (strain) coefficient for each linear regression model, and are reported for $p<0.05$.

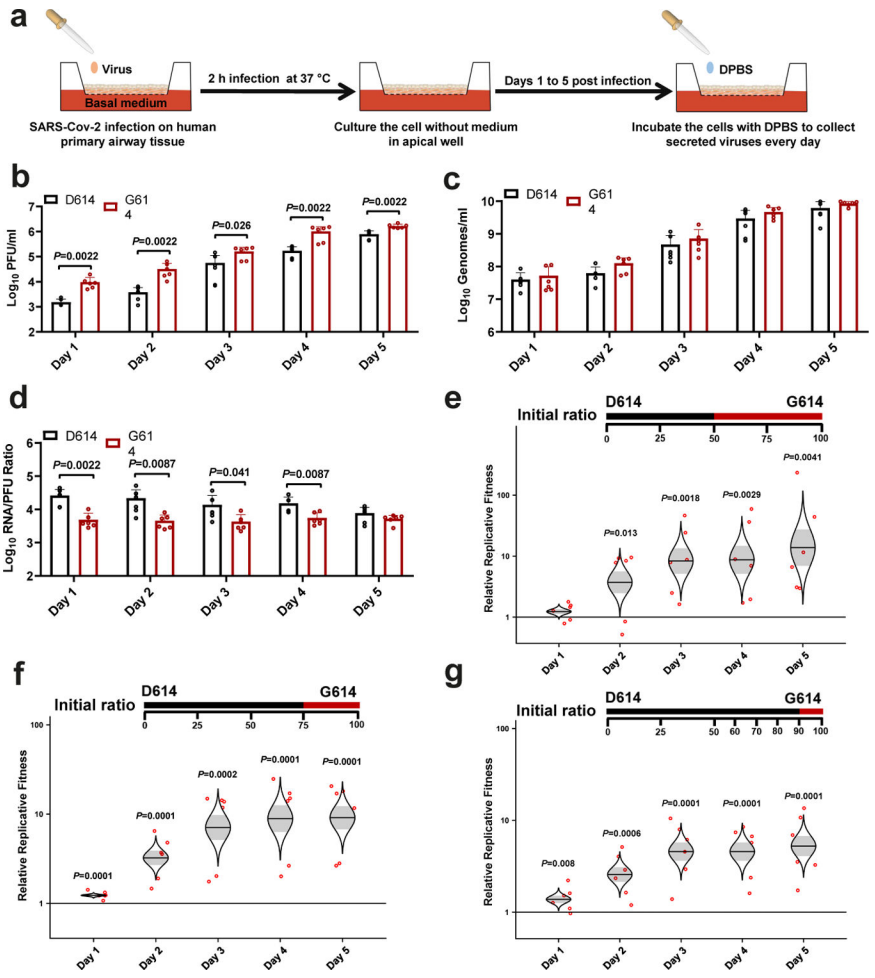

Figure 3. D614G substitution significantly enhances SARS-CoV-2 replication in primary human airway tissues.

(a) Experimental scheme. D614 and G614 viruses were inoculated onto the primary human airway tissues at an MOI of 5. After incubation for 2 h, the culture was washed with DPBS, then maintained at for 5 days. To harvest, DPBS was added and allowed to incubate at 37°C for 30 min to elute the virus. **(b-d)** Viral replication and genomic RNA/PFU ratios. The amounts of infectious virus (b) and genomic RNA (c) were quantified by plaque assay and real-time RT-qPCR, respectively. The genomic RNA/PFU ratio (d) was calculated to indicate virion infectivity. Symbols represent individual samples, bar heights represent means, and error bars represent standard deviations. *P* values were determined by two-tailed Mann–Whitney test (n=6, two independent experiments conducted in triplicate). The results of the Mann-Whitney test are reported for all instances of $p<0.05$. **(e,f)** Competition assay. A mixture of D614 and G614 viruses with initial ratios of 1:1 (e), 3:1(f), or 9:1(g) were inoculated onto the human airway tissues at a total MOI of 5. Ratios after competition were measure by Sanger sequencing. Circles represent individual samples (n=6, two independent experiments conducted in triplicate). The midline represents the sample mean, and the shaded region represents +/− one unit of standard error about the mean. The width of the catseye plot represents the distribution of the model-adjusted means, and the heights extend to span 99.8% of the distribution of the mean. The y-axis is displayed on the $\log_{10}$ scale such

that the null value is 1. P values are calculated for the group (strain) coefficient for each linear regression model, and are reported for all instances of $p<0.05$.

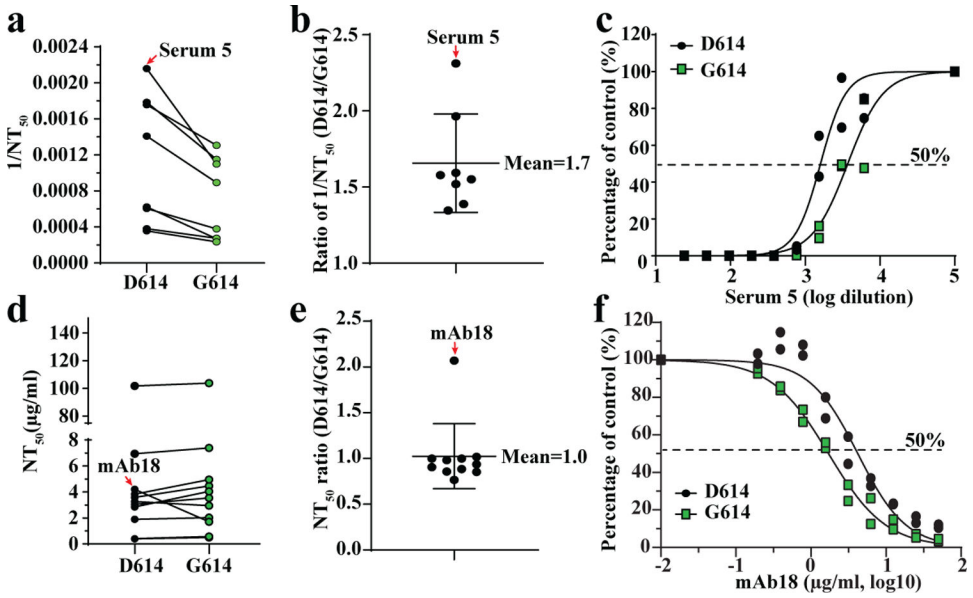

Figure 4. D614G substitution affects the neutralization susceptibility of SARS-CoV-2.

(a) Neutralizing activities of hamster sera against D614 and G614 mNeonGreen reporter SARS-CoV-2. Sera from D614 virus-infected hamsters (n=8) were tested for neutralizing titers against D614 and G614 reporter SARS-CoV-2, and the $1/NT_{50}$ values are plotted. Symbols represent sera from individual animals. **(b)** Ratio of $1/NT_{50}$ between D614 and G614 viruses. Symbols represent sera from individual animals (n=8), the midline represents the mean, and error bars represent standard deviation. **(c)** Representative neutralizing curve of hamster serum 5. Symbols represent individual replicates, the solid line represents the fitted curve, and the dotted line indicates 50% viral inhibition. **(d)** Neutralizing activities of eleven human mAbs against D614 and G614 mNeonGreen SARS-CoV-2. Symbols represent individual mAbs. The data represents one of the two independent experiments. **(e)** Ratio of NT_{50} between D614 and G614 viruses. The averages of the NT_{50} ratios from two independent experiments performed in duplicates are shown. Symbols represent individual mAbs, the midline represents the mean, and the error bars represent the standard deviation. **(f)** Representative neutralizing curve of mAb18. Symbols represent individual replicates, the solid line represents the fitted curve, and the dotted line indicates 50% viral inhibition.